2005-01-31

Energimyndigheten

Titel: Hygroscopic behaviour of aerosol particles emitted from biomass fired grate boilers

Författare:	Jenny Rissler	Div. of Nuclear Physics, Lund University
	Joakim Pagels	Div. of Ergonomics and Aerosol Technology, Lund University
	Erik Swietlicki	Div. of Nuclear Physics, Lund University
	Aneta Wierzbicka	Div. of Ergonomics and Aerosol Technology, Lund University
	Michael Strand	Bioenergy Technology, Växjö University
	Lena Lillieblad	”-
	Mehri Sanati	”-
	Mats Bohgard	Div. of Ergonomics and Aerosol Technology, Lund University

RAPPORT INOM OMRÅDET BIOENERGI/KLIMAT

Rapportnummer: BIOK 05/6

Projektledare: Erik Swietlicki

Projektnummer: P21848-1

Projekthandläggare på Statens Energimyndighet: Irene Wrande

Box 310 • 631 04 Eskilstuna • Besöksadress Kungsgatan 43
Telefon 016-544 20 00 • Telefax 016-544 20 99
stem@stem.se • www.stem.se
Org.nr 202100-5000

2005-01-31

Energimyndigheten

Rapportnummer: BIOK 05/6

Sammanfattning:

This study focuses on the hygroscopic properties of sub-micrometer aerosol particles emitted from small-scale local district heating combustion plants (1-1.5 MW) burning two types of biomass fuels (moist forest residue and pellets). A method was presented that allows for a calculation of the fractal dimension (and size-dependent shape factor) of agglomerated combustion aerosols. The particle water uptake (after correction for particle shape) could be adequately explained by the Zdanovskii-Stokes-Robinson (ZSR) mixing rule with particles consisting purely of potassium salts.

Box 310 • 631 04 Eskilstuna • Besöksadress Kungsgatan 43
Telefon 016-544 20 00 • Telefax 016-544 20 99
stem@stem.se • www.stem.se
Org.nr 202100-5000

Hygroscopic behavior of aerosol particles emitted from biomass fired grate boilers

Jenny Rissler[1], Joakim Pagels[2], Erik Swietlicki[1], Aneta Wierzbicka[2], Michael Strand[3], Lena Lillieblad[3], Mehri Sanati[3], Mats Bohgard[2]

[1]Div. of Nuclear Physics, Lund University, P.O. Box 118, SE-22100, Lund, Sweden
[2]Div. of Ergonomics and Aerosol Technology, Lund University, P.O. Box 118, S-22100, Lund, Sweden
[3]Bioenergy Technology, Växjö University, SE-35195, Växjö, Sweden

Corresponding author: Jenny Rissler, jenny.rissler@nuclear.lu.se

Running title: Hygroscopicity of biomass combustion particles

Abstract

This study focuses on the hygroscopic properties of sub-micrometer aerosol particles emitted from two small-scale district heating combustion plants (1 and 1.5 MW) burning two types of biomass fuels (moist forest residue and pellets). The hygroscopic particle diameter growth was measured when taken from a dehydrated to a humidified state for particle diameters between 30-350 nm (dry size) using a Hygroscopic Tandem Differential Mobility Analyzer (H-TDMA). Particles of a certain dry size all showed similar hygroscopic growth and the average diameter growth at RH=90% for 110/100 nm particles was 1.68 in the 1 MW boiler, and 1.52 in the 1.5 MW boiler. These growth factors are considerably higher in comparison to other combustion aerosol particles such as diesel exhaust, and are the result of the efficient combustion and the high concentration of alkali species in the fuel. The observed water uptake could be explained using the Zdanovskii-Stokes-Robinson (ZSR) mixing rule and a chemical composition of only potassium salts, taken from an Ion Chromatography analysis of filter sample (KCl, K2SO4, and K2CO3). Agglomerated particles collapsed and became more spherical when initially exposed to a moderately high relative humidity. When diluting with

hot particle-free air, the fractal-like structures remained intact until humidified in the H-TDMA. A method is presented to by which to estimate the fractal dimension of the agglomerated combustion aerosol and correct the measured mobility diameter hygroscopic growth to the more useful property volume growth. The fractal dimension was estimated to be ~2.5.

Introduction

The supply of energy is one of the main issues in today's energy consuming society. Due to the increasing CO_2 concentrations in the atmosphere, authorities strive to decrease the usage of fossil fuels. As a consequence, the use of renewable and CO_2-neutral energy sources is predicted to increase in the forthcoming years. Sweden is one country amongst other with a potential to increase the energy production from biomass burning. Today bio-fuels are contributing to about 16% (98 TWh, Energy in Sweden, 2003) of the total energy supply, increasing by ~4 TWh annually. The use of bio fuels is expected to increase, with a significant proportion invested in plants between 0.5 and 10 MW using moving grate techniques.

Biomass combustion emits large amounts of both fine and coarse particles, if no particle removal technique is utilized. There is now a general consensus that elevated concentrations of both PM_{10} (mass concentration of particles with an aerodynamic equivalent diameter < 10 μm) and $PM_{2.5}$, are associated with adverse health effects (WHO, 2003; WHO, 2004). In the EU member states, this has resulted in new air quality limit values being adopted for PM_{10}, to come into effect from 1 January 2005 (Council Directive 1999/30/EC). The EU limit values for PM are currently being re-evaluated, and they are likely to be followed also by limit

values for $PM_{2.5}$ (WHO, 2003). Although the exact mechanisms of the health effects are not known, chemical composition, size, morphology and solubility are likely to be important parameters.

Aerosol particles emitted from combustion of biomass can also have impact on regional and global climate through their influence on Earth's radiation budget and cloud microphysics. The role of atmospheric aerosols on cloud formation and lifetime (the indirect effect of aerosols on climate) and thereby the global radiation balance currently constitutes the largest source of uncertainty in our ability to predict future climate change resulting from human activities (IPCC, 2001).

It is important to investigate the scale of the increasing emissions by biomass combustion and to determine the characteristics of emitted particles in order to tackle the associated problems.

Several previous studies have been carried out on particle formation and emissions from woody biomass combustion for heat and power production. These range from large scale (25-100 MW) CFB (Circulating Fluidised Bed)-boilers (Valmari et al. 1999), grate-combustion in 0.5-12 MW boilers (Pagels et al. 2003; Lillieblad et al. 2004) to small (10-20 kW) residential wood stoves and boilers (Hedberg et al. 2002; Johansson et al. 2004). Also other biomass combustion fuels have been considered for energy production as for instance straw (Christensen et al. 1998) and olive residues (Jimenez et al. 2004), as well as co-firing of biomass and fossil-fuels. Biomass burning in the open resulting from wild-fires and deforestation have also attracted attention (Reid et al. 2003 and Andreae and Merlet, 2001). During favorable combustion as e.g. in the CFB-boilers, ash components like K_2SO_4, KCl and in some cases K_2CO_3 dominate the fine particle composition. Potassium is volatilized during

combustion, and contributes to the formation of particles by homogeneous nucleation and subsequent condensation as the flue gases cool down. K_2SO_4(s) will start to form already at around 1000 °C, with KCl(s) condensing on the existing particles at lower temperatures (~650 °C). The concentration of these ash components is mainly governed by the inorganic content of the fuel. For instance, particle emissions from bark fuels have relatively high K_2SO_4 content, while particles from straw fuels have higher KCl content. Several environmentally or health relevant metals present in the fuel, such as Zn, Cd, and Pb, may be enriched in the fine particles by similar mechanisms i.e. gas to particle conversion. If the combustion conditions are poor – as might be the case in forest fires and during the start-up phase in residential boilers –products of incomplete combustion containing carbon may dominate the chemical composition. Elemental Carbon (EC i.e. soot) is formed at high temperatures in fuel-rich regions and may be emitted when oxidation is not complete. Organic carbon (OC) compounds are generally volatile and condense at lower temperatures. The composition of fine particles from biomass combustion covers the full spectrum from almost pure KCl /K_2SO_4 particles in CFB boilers to almost pure OC/EC particles in forest fires. Although not studied in detail, the relative abundance of these two classes of particle-components is expected to vary strongly over the combustion cycle. Some information is available on the variation in inorganic composition on a particle-by-particle basis from electron microscopy-EDX analysis (Brunner et al. 2001), but more studies are needed to better understand the mixing status.

The aim of this study was to investigate the hygroscopic properties of the flue gas particles emitted from biomass-fired district heating units, using a Hygroscopic Tandem Differential Mobility Analyzer (H-TDMA). Hygroscopic properties in this study relate to how the particles absorb water vapor and grow into droplets as a function of the relative humidity (RH).

The hygroscopic properties of aerosol particles are important for several reasons. As mentioned above, the fine particles can give adverse health effects when deposited in the human airways. The deposition pattern and deposition probability in the respiratory system is strongly dependent on the particle size in the actual airways. In the lower respiratory tract the equilibrium RH is about 99.5% (Anselm 1990). Under these conditions NaCl particles grow by a factor of five to six in diameter. The sub-micrometer particles might also have a large impact on climate through changing the radiation budget and cloud processes. Particle hygroscopic growth is a crucial parameter for light scattering and for the selection of the sub-population of particles that act as cloud condensation nuclei (CCN). Furthermore, the measurements of hygroscopic properties can provide highly size and time-resolved information regarding the mixing status of the aerosol and as well as proxy data on the chemical composition of the particles. In the case of biomass combustion aerosols, these properties can be used for a better understanding of particle formation processes as well as to develop more efficient cleaning techniques.

Water vapor uptake of biomass combustion aerosol particles can be either due to the presence of water-soluble salts (mostly potassium salts) or due to the presence of water-soluble organic compounds. As an example, pure KCl has a diameter growth factor of around 2 at RH=90%. A large fraction of the water-soluble OC in biomass smoke consists of partly oxidized compounds originally present in the fuel. These compounds typically have lower growth factors. One abundant compound in biomass burning aerosol particles is levoglucosan – a pyrolysis product of cellulose (Simoneit et al. 1999) – which has a growth factor of around 1.3 at 90% RH (Svenningsson et al. *To be submitted to ACPD*).

Previously, only few measurements on hygroscopic diameter growth of biomass burning aerosols have been reported, some with regard to natural forest fires or clearing forest in the Amazon region (Rissler et al. 2004, Vestin et al. 2004), laboratory-scale experiments burning peat (Chand et al. 2004) and indoor small-scale fires (Dua and Hopke, 1996). Field studies of biomass burning smoke aerosol in Amazonia report low hygroscopic growth factors (~1.1-1.3) at 90 % RH (Vestin et al. 2004). For the laboratory-scale experiment burning peat the hygroscopic diameter growth, measured at 85% RH, was 1.04, corresponding to a growth of ~ 1.06 at 90% RH (for 80 nm particles). For the indoor small-scale fires, measured at 99% RH, the growth was ~1 for an open flame fire and 2 for particles from a smoldering fire, corresponding to a growth of ~ 1-1.35 at 90% RH. The hygroscopic growth of ambient particles in Pasadena, California, US increased during a period of nearby forest fires (Crocker et al. 2001). The differences in results are probably due to highly variable burning conditions and combustion efficiency. To our knowledge no measurements on hygroscopic diameter growth have been reported from biomass combustion in biomass-fired district heating units, where the combustion conditions are favorable and water-soluble potassium salts tend to dominate the particle composition.

Combustion particles may be highly agglomerated. Park et al. (2004) have reported that the dynamic shape factor of diesel soot increased from 1.1 to 2.2 over the size-range 50-220 nm. Spark-discharge carbon particles, and to a smaller extent diesel soot particles, restructure to more compact particles already at relatively low RH due to the inverse Kelvin effect (Weingartner et al. 1997). Krämer et al. (2000) used a H-TDMA to show that NaCl-particles generated with an evaporation-condensation method were highly agglomerated and already at RH significantly below the deliquescent point particle compaction occurred. Dynamic shape factors assessed from mobility changes and hygroscopic growth models were on the order of

4-5. Mavrocordatos et al. (2002) used an Atomic Force Microscope and Transmission Electron Microscopy to analyze the morphology of fine particles from pellets combustion. They found agglomerated particles and single monomers. The particles became more compact after exposure to water.

In this study hygroscopic growth measurements are presented from two biomass-fired heating plants, situated in Southern Sweden. The Zdanovski-Stokes-Robinson (ZSR) method were used to predict hygroscopic growth from the chemical composition. The chemical composition was evaluated from low-pressure cascade impactor and filter samples using IC (Ion Chromatography) and PIXE (Particles Induced X-ray Emission). A method is presented that here can be used to estimate the fractal dimension of the highly agglomerated combustion aerosol and correct the measured mobility diameter hygroscopic growth to the more useful property volume growth. Furthermore, parallel measurements of the aerosol particle size distribution were performed with an electrical mobility spectrometer and an electrical low-pressure impactor.

2. Methods and theory

2.1 Combustion system and particle sampling

The measurements were carried out in two biomass fired moving grate boilers, used for local heat production, situated in the southern part of Sweden. The two boilers are a 1 MW boiler operating on moist forest residues (boiler 1) and a 1.5 MW boiler fired with dry pellets (boiler 2). During the measurements the boilers were operated at 45-100% and 20-50% load, respectively.

The flue gas was sampled isokinetically downstream the multi-cyclone (the only flue-gas cleaning device installed) and two different dilution systems were in use. For boiler 1 (the 1 MW boiler) the flue gases were diluted (1:10) and cooled to room temperature using particle-free dry compressed air at ambient temperature. In this system the flue-gas sample experienced a high RH during dilution, which may to some extent simulate the dilution in and after the stack. The cooled gas stream was further diluted (1:10) before being sampled. For boiler 2 (the 1.5 MW pellets boiler) a heated two-stage ejector based dilution system was used. The first dilution stage used heated (110 °C), particle free air. This type of dilution system is often used in biomass combustion studies and prevents condensation of water and volatile components on the particles. The boilers and the sampling systems are described in more detail by Pagels et al. (2003) and Wierzbicka et al. (2004). All concentrations are normalized to 13% CO_2, at 0°C and 101.3kPa.

2.2 Hygroscopic measurements

2.2.1 Principle of the H-TDMA

The hygroscopic properties of sub-micrometer aerosol particles were studied with a H-TDMA. The selected particle dry sizes were in the range between 20 and 350 nm. The size-classified dry quasi-monodisperse particles were humidified, and the altered wet size distribution was determined. From this, the diameter growth factor was determined. The DMA's used are of Vienna-type (Winklamyr et al. 1991).

In principle the H-TDMA consists of three parts; a Differential Mobility Analyzer (DMA1) that selects a narrow, quasi-monodisperse size fraction of dry (RH<10%) particles from the sampled aerosol, humidifiers conditioning the aerosol to a controlled humidified state, and a second DMA (DMA2) that measures the change in size caused by the imposed humidification. The aerosol and the sheath flows entering DMA2 were humidified separately.

The H-TDMA was operated in two different modes: 1) the size-scanning mode and 2) the RH-scanning mode. Using mode 1 the humidity is kept constant while the selected dry size in DMA1 is varied. This gives information of how the hygroscopic behavior of the aerosol changes with particle size. Mode 2 instead keeps the selected dry size while scanning the RH, here between 20-90%. This can be used to evaluate the deliquescent behavior of the aerosol particles.

A more detailed technical description of the H-TDMA can be found in Svenningsson (1997) and Zhou (2001).

2.2.2 Quality assurance

The H-TDMA data is evaluated and assured for quality off-line, using a number of parameters logged by the H-TDMA software. Certain criteria on the variations in concentration, RH and temperatures had to be fulfilled for data to be accepted. These criteria were used when calculating the instrumental error in Figure 7.

To determine the RH in the second DMA, a dew point hygrometer placed in the excess air of DMA2, together with temperature sensors placed before, after and outside the DMA2 were used. In order to secure the performance of the system as well as to determine the RH (i.e. temperature) with as high accuracy as possible, the hygroscopic growth of a standard aerosol of pure ammonium sulfate was measured and compared to the modeled growth using the parameterizations of Tang and Munkelwitz (1994), and Gysel et al. (2002). For a more extensive description of the quality assurance procedure, see Rissler et al. (2004) and Swietlicki et al. (2000).

During the measurements in boiler 1, the H-TDMA instrument was somewhat unstable, leading to larger errors in RH than in the measurements at boiler 2. This was taken into account in the estimation of errors, and these are shown together with data in Figure 7.

2.2.3 Data processing

Each spectrum of the humidified aerosol size distribution was fitted with a computer program (Zhou, 2001) based on the theory and algorithm of "TDMAFIT" (Stolzenberg and McMurry 1988). This program estimates the arithmetic mean diameter growth factor (defined as the ratio between the conditioned and dry particle diameter), the diameter growth dispersion factor (the broadening in addition to ideal TDMA transfer function), and the number fraction of particles in each fitted hygroscopic particle group.

Despite considerable efforts to stabilize the RH in DMA2, deviations from the nominal RH are difficult to avoid during operation. In order to study the variation in hygroscopic behavior with respect to size, the temporal variations, and facilitate comparisons between the two boilers, the growth factors of the size-scans were corrected from the actual DMA2 RH to the nominal RH (here 90%). The salt used for this RH correction was KCl (Tang 1997), which according to the IC-analysis is one of the dominating inorganic salts of the investigated particles. The corrections were made as described by Swietlicki et al. (2000). Since the accepted variation in DMA2 RH is relatively small, the dependence on the type of salt applied in this correction is small.

Each hygroscopic growth distribution was fitted with 1-3 modes. Even though the hygroscopic growth and the modal structure sometimes changed rapidly, the hygroscopic

growth distribution was mostly dominated by one mode, the multiple modes were often close in growth when being separated. The average growth factor of each distribution is presented in Table 1. To present the broadening, which is related to the mixing status of the particles, an interval of the hygroscopic growth factor covering 95 % of the wet distribution (of the fitted distribution) of the selected quasi-monodisperse aerosol is given.

2.3 Additional measurements

A Scanning Mobility Particle Sizer (Wang and Flagan, 1991) was operated in parallel with the H-TDMA during the two experiments. In addition, a Dekati 13-stage multi-jet low-pressure cascade impactor (LPI) was used to collect samples for gravimetric analysis, elemental analysis (PIXE), and analysis of major ions (IC). An Electrical Low-Pressure Impactor (ELPI; Marjamäki et al. 1999) was used in the second boiler. These measurements are described in more detail by Pagels et al. (2003), Lillieblad et al. (2004) and Wierzbicka et al. (2004).

2.4 Hygroscopic growth and the ZSR mixing rule

The water uptake of a particle containing a chemical compound can be described using the Köhler equation (Köhler 1936). The Köhler equation combines the Kelvin curvature effect (C_k) and Raoult's law for water activity (a_w) as:

$$\frac{RH}{100} = C_k \cdot a_w = \exp\left(\frac{4M_w\sigma}{RT\rho d_a}\right) \cdot \frac{1}{1+\nu \cdot M_w \cdot m_s} \quad , \qquad (1)$$

where M_w is the molar weight of water, σ the surface tension, R the universal gas constant, T the temperature in Kelvin, ρ the solution density, d_a the droplet diameter, ν the number of dissociating ions per molecule and m_s the molality of the solute (moles of solute per kilogram of water). At subsaturations this equation describes the equilibrium size of the droplet at a

certain RH. The first term in the Köhler equation takes into account the increase in equilibrium water vapor pressure caused by the droplet curvature, often called the Kelvin curvature effect, and the second term describes the depression in water vapor pressure due to soluble material in the particles, the Raoult's solution effect. Over a flat surface a_w is equal to RH ($C_k=1$). When using a_w instead of RH, the effect of particle size is removed and only the only Raoult's effect is considered. For example, at a_w=0.9 particles of identical chemical composition grows the same. The smaller particles have a lower equilibrium size since a stronger curvature increases the equilibrium water vapor pressure (C_k).

The Köhler equation written in the form above describes the ideal growth of a droplet. However, most solutions are not ideal, i.e. they do not strictly obey Raoult's law. Their non-ideal behavior can be described using several different approaches such as introducing the van't Hoff factor (substituting the number of soluble ions in eq. 1), the osmotic coefficient, or to any other parameterization of the measured water activity as a function of solute molality. The non-ideal parameters are most often determined experimentally.

2.4.1 The Zdanovski-Stokes-Robinson (ZSR) method

A relatively simple way of estimating the hygroscopic growth of mixtures is to use the Zdanovski-Stokes-Robinson (ZSR) method (Stokes and Robinson, 1966). The ZSR method is defined by the equation:

$$1 = \sum \frac{m_s(a_w)}{m_{o,s}(a_w)} \qquad (2)$$

where m_s is the molality of the compound s in the mixture, and $m_{o,s}$ the molality of the single electrolyte solution of the component s, for which the water activity equals that of the solution mixture. This can also be expressed as a summation of the water mass ($mass_{w\_s}$) associated

with the amount of the single electrolyte present in the mixed particles at a given water activity,

$$mass_{w\_tot} = \sum mass_{w\_s} \quad (3)$$

where $mass_{w\_tot}$ is the water mass in the mixture at a given water activity (Svenningsson et al. *To be submitted to ACPD*).

2.4.2 Pure salts

To calculate the hygroscopic growth using the ZSR method, the hygroscopic growth of the pure compounds needs to be known. The main components of the biomass combustion aerosol studied here were K_2SO_4, K_2CO_3 and KCl. Since no data was found for the hygroscopic growth of K_2CO_3, this salt was further investigated in laboratory H-TDMA measurements. KCl has been characterized by Tang et al. (1997). They measured the water activity (a_w) down to the point of crystallization (a_w = 0.62-1). For K_2SO_4, water activity data from in Guendouzi et al. (2003) was used. However, they only measured the water activity for non-supersaturated (bulk) solutions. No water activity data was found for supersaturated solutions of K_2SO_4. Since the solubility of K_2SO_4 is low (0.12 g/cm^3, from Lide, 1991) the deliquescence point is around a_w ~0.97. The high deliquescence point makes it impossible to measure the deliquescent branch using our H-TDMA system. In order to estimate the hygroscopic growth below the point of deliquescence, we use the fact that the hygroscopic growth for particles consisting of non-ideal subsaturated solutions can be approximated from classical Köhler theory, substituting the number of dissociating ions by a constant van't Hoff factor. As a result of the variable degree of dissociation and non-ideal interactions in the electrolyte, the van't Hoff factor varies with molality. While this may be crucial when estimating the activation of particles into cloud droplets at water vapor supersaturation, a constant van't Hoff factor is often a satisfactory approximation at subsaturation (RH < 100

%). In the interval measured by Guendouzi et al. (2003) (a_w = 0.972-0.9958), a van't Hoff factor of 2.05 can for our purpose adequately describe the measured water activity. This value was used in equation 1 to extrapolate the hygroscopic behavior of K_2SO_4 down to supersaturated solutions.

2.4.3 Solubility

The solubility must be taken into account when using the ZSR mixing rule for compounds with limited solubility. This is the case for K_2SO_4 and partly also for KCl. In Svenningsson et al. (*To be submitted to ACPD*) this was made assuming the particles go partly into solution if other salts provide the water liquid phase, an assumption also used here. The water accessible for the solution is assumed to be $V_{droplet}$-$V_{non\text{-}soluble\,fraction}$, where $V_{droplet}$ is the droplet volume and $V_{non\text{-}soluble\,fraction}$ is the volume of the not yet dissolved fraction of the particle. The solubilities are calculated from the solubility products, K_{sp}, and takes into account the common-ion effect, i.e. that the solubility of one potassium salt is affected by the presence of the other potassium salts (McMurry and Fay, 1998). The solubility products used are calculated from the solubility of the pure salts taken from Lide (1991). The solubilities of the pure compounds (and the solubility products) are 1.12 g/cm^3 (2129 mol^3/dm^9) for K_2CO_3, 0.344 g/cm^3 (21.3 mol^2/dm^6) for KCl, and 0.12 g/cm^3 (1.31 mol^3/dm^9) for K_2SO_4.

2.5 Fractal dimension

When dealing with freshly emitted combustion aerosols, the particles can be highly agglomerated. For particles of equal mass, the mobility diameter is larger for particles of a non-spherical shape. This is described by adding the dynamic shape factor, χ, to Stokes law (e.g. Hinds 1999),

$$\frac{d_{mobility}}{C_c(d_{mobility})} = \chi \cdot \frac{d_{ve}}{C_c(d_{ve})} . \quad (4)$$

Here d_{ve} is the volume equivalent diameter, $d_{mobility}$ the mobility equivalent diameter and C_c the Cunningham slip correction factor. Note that when water condenses on an agglomerate particle it may start to restructure to a more compact shape due to the inverse Kelvin-Effect (Weingartner et al. 1997), thus possibly lowering the mobility diameter.

For agglomerated particles formed by coagulation, the mass-fractal dimension *Df*, is often used. *Df* is a parameter linking radius (length scale) and mass over a certain size range, defined as

$$m = C_2 \cdot r_g^{Df} , \quad (5)$$

where r_g is the agglomerate's radius of gyration, m is the mass of the agglomerate and C_2 a constant. The radius of gyration is defined as the average distance from aggregate center of mass to each primary particle. This relation has been well established to describe fractal like agglomerates grown in diffusion-limited processes, in both simulations and experiments (Schmidt-Ott et al. 1990). According to Schmidt-Ott et al. (1990) the relation between the radius of gyration and the mobility diameter is linearly proportional in both the continuum regime and the free molecular regime, (for fractal dimensions $Df>2$). No population is however strictly fractal.

The present measurements were made in the intermediate regime, but a population of particles having coagulated under the same conditions will most often not have size distributions broader than the size range where *Df* is expected to be approximately constant, (Schmidt-Ott et al. 1990).

The mass of an aerosol particle can also be expressed as

$$m = \rho_{bulk} \cdot \frac{\pi}{6} \cdot d_{ve}^3, \quad (6)$$

where ρ_{bulk} is the inherent material density of the particle material. Consequently (from eq. 5) d_{ve}, r_g and d_{me} are related as:

$$r_g^{Df} \propto d_{me}^{Df} \propto d_{ve}^3. \quad (7)$$

The mass of the agglomerated particles is scaled by d_{me} raised to Df instead of 3. As a consequence, larger particles in the same population have a more open structure and higher dynamic shape factors.

2.5.1 Fractal dimension in H-TDMA measurements

In the H-TDMA, particles of a certain dry mobility diameter are selected and humidified. When humidified enough, the hygroscopic agglomerates become spherical droplets (d_{me}=d_{ve}). Calculating the diameter growth factor (Gf), defined as the ratio between wet d_{ve} and the dry d_{ve}, often the dry size is approximated by the measured d_{me}. In the case for processed atmospheric aerosols this is an approximation that most often is not introducing large errors. However, for freshly emitted combustion aerosol particles the errors introduced doing such an approximation can be large. In order to correctly link the condensed water volume to the volume of the dry particle for an agglomerated aerosol (Df<3), the relation in equation 7 can be used and the hygroscopic growth factor should be calculated according to.

$$Gf = \frac{d_{ve}(90\%RH)}{d_{ve}(10\%RH)} = \frac{d_{wet}}{\sqrt[3]{d_{me\,dry}^{Df}}} \cdot C_3. \quad (8)$$

d_{wet}, is the humidified diameter and $d_{me\,dry}$ the selected dry size in DMA 1. C_3 is a constant, which depends on the particle shape of the smallest considered particles.

Assuming a constant chemical composition of the aerosol particles within a certain size range, the fractal dimension determines the change in the measured ratio between d_{wet} and $d_{me\,dry}$ relative (and *Gf* not taking the shape of the particles into account). That is if subtracting the Kelvin curvature effect, the growth for an aerosol with a chemical composition constant over size should also be constant over size. The fractal dimension explains the decrease in growth and can accordingly be estimated from H-TDMA data.

When estimating the fractal dimension, the hygroscopic growth of a model salt of the same wet size as the measured (to take into account the Kelvin curvature effect) was calculated. The fractal dimension as well as C_3 were then fitted, changing the volume equivalent dry diameter of the measured particles, until the hygroscopic behavior of our measurements showed the same hygroscopic behavior as the model salt.

The fractal dimension is not dependent on the absolute measured growth, but on the relative change in the ratio between d_{wet} and $d_{me\,dry}$. This makes the calculation almost independent of which salt that is used in the calculation. Still there is a small dependence due to the non-ideal behavior of most salts (deviations from Raoult's law) as well as the non-linear dependence between the hygroscopic growth and the number of soluble ions in each particle.

3. Result and discussion

3.1 Time and Size-resolved analysis of concentrations

Size-distribution data from the two boilers have been described in more details previously (Pagels et al. 2003 and Wierzbicka et al. 2005). Total number concentration (normalized to 13% CO_2 and NTP) of emitted particles was $5.1 \cdot 10^7$, $6.3 \cdot 10^7$ and $2.9 \cdot 10^7$ particles/cm^3 for 50 and 100% load in boiler 1 and 30% load in boiler 2, respectively. All size-distributions were

essentially unimodal with a weak shoulder at around 40 nm in boiler 1 (Figure 1). The geometrical mean diameter of fitted log-normal size-distributions were 117, 90 and 77 nm. The size-distributions were in principle stable over time, with the exception of the largest particles in boiler 2. In Figure 2, the relative standard deviation (coefficient of variation) in time of the concentration in each SMPS size-channel is given. Only sizes for which the variations due to counting statistics are less than 20% of the given standard deviation are included. The relative standard deviation is significantly larger than 0.2 only for particles larger than 150 nm in boiler 2 and particles below 50 nm at the lower load in boiler 1.

The time variations in boiler 2 were studied in more detail using an ELPI, for which a new size distribution was saved every 10 seconds. Figure 3 shows the time variations in detail for a representative period of 30 minutes given as detected current for stage 3 (d_{ae}=128 nm), 5 (d_{ae}=311 nm) and 6 (d_{ae}=494 nm). Often there was a clear periodicity in the time-variations, typically on the order of 1 min likely caused by grate-movements. Note that the SMPS has too low time-resolution (2 min in boiler 2) to detect these fast changes in concentration. These particle sizes may have different formation mechanisms and chemical composition.

Sub-micrometer mass size distributions, gravimetrically determined, had single mode with peaks in aerodynamic diameter around 200 to 300 nm. PM_1 concentrations were around 120 mg/m^3 and 40 mg/m^3 in boiler 1 and 2, respectively. The higher concentration in boiler 1 is due to the higher alkali content in the forest residue fuel. The variations in time for larger sizes in boiler 2 had little effect on the number concentration as is evident in Figure 1, but affected considerably the mass concentration.

3.2 Size-resolved chemical composition

Size-dependent information about the chemical composition is needed for comparison and interpretation of the hygroscopic properties measured on-line with the H-TDMA. Water-soluble ions detected by Ion-chromatography are given in Figure 4 as ion equivalent concentrations. The dominating ions were K_2SO_4, K_2CO_3 and KCl in boiler 1 and K_2SO_4 and KCl in boiler 2. Also present were traces of Na, Mg and Ca. The fraction of K_2CO_3 was estimated from an excess of positive ions found in the IC analyses (Pagels et al. 2003). With PIXE, the variations in inorganic composition with size could be studied in more detail. The sulfur to chlorine mass ratio increased with particle size in boiler 1, while in boiler 2 the S/Cl ratio was essentially independent of particle diameter (Figure 5). We used the detected composition from IC as input to predict the hygroscopic growth with the ZSR rule. For boiler 1 a sensitivity test of the hygroscopic growth due to the size-dependent S/Cl ratio was made. The ratios were taken from the PIXE measurements.

The increasing Cl/S ratio for smaller particles seen in boiler 1 was possibly because KCl condenses later in the combustion process compared to K_2SO_4, and then mostly influences the composition of the smallest particles. The reason for the difference between boiler 1 ad 2 is not known.

The fraction of the gravimetrically determined mass detected by IC for boiler 2, decreased from about 0.70 in stages 2 and 3 (77 and 133 nm) to around 0.25 in stages 5 and 6 (323 and 510 nm). The detected fractions for both PIXE and IC increased to 0.50 for particles larger than 700 nm. However, neither PIXE nor IC can detect carbon. Wierzbicka et al. (2004) analyzed PM_1 samples for organic (OC) and elemental carbon (EC) in boiler 2 during the

same measurement campaign. They found that OC and EC contributed to on average 8 and 34% of PM_1 respectively. The EC concentration varied by a factor of three in 4 different samples. The estimated SMPS mass-concentration (assuming constant effective density) in the range 250-320 nm was highly correlated (r^2=0.99) with the EC concentration in individual samples. The correlation was significantly lower for 150-250 nm (0.66) and 25-150 nm particles (-0.28).

The results above make it likely that EC is enriched in particles between 150 and 700 nm. This is also in line with the observed fast temporal variations in concentrations observed with both ELPS and SMPS for particles d_{ae}>150 nm. Measurements of Organic Gas-phase Carbon (OGC) showed a low baseline value (<1 ppm, dry gas) with high peaks above 10 ppm occurring several times per hour. Unfortunately ELPI and OGC-measurements were not performed simultaneously in boiler 2. However, the analysis of a data-set from a similar boiler operated on sawdust showed that the mass estimated as PM_1 from ELPI measurements was highly correlated with both OGC and CO-measurements (Szpila et al. 2003). It is likely that the EC is emitted at high concentrations during periods of high OGC emissions. Inorganic salts are continuously evaporated and form smaller particles, for which the temporal variations were small in both boilers.

In boiler 1, the fast temporal variations were low for particle diameters between 150 to 400 nm. The total PAH-concentration (particle and gas phase) of 29 analyzed compounds (Lillieblad et al. 2004) was very low (2.8 $\mu g/m^3$). OGC-measurements showed a very low baseline and peaks never exceeded 3 ppm during the measurement. Therefore we expect the carbon contribution in boiler 1 to be negligible.

It should be noted that the chemical analysis reported here was done off-line with poor time-resolution. Single mean values of the chemical composition were used to predict the hygroscopic properties for the whole measurement campaign in each boiler.

3.3 Hygroscopic properties

In this section the hygroscopic behavior of the flue-gas particles emitted from each unit will be presented together with a short comparison and discussion of the results.

3.3.1 Boiler 1: 1 MW boiler fired with moist forest residues

During the measurements the boiler was running either at 50% or 100% load. The primary dilution (1:10) of the flue gases was made with dry compressed air at ambient temperature, leading to a higher relative humidity and possibly to a restructuring of agglomerate particles in the dilution system.

RH scan

In the 1 MW unit RH scans were performed for 120 and 200 nm particles at around 50% boiler load. The particles started to take up water already at low RH. No shrinking behavior and no clear deliquescent point was seen. The result is shown in Figure 6. The measurements do not show any indication of fractal-like behavior of the investigated particles.

The absence of deliquescent point is not surprising. Aerosol particles consisting of a mixture of many compounds, as for atmospheric aerosols, often display a continuous hygroscopic growth without deliquescence steps. The deliquescence point for pure K_2SO_4 is a_w~0.97 (estimated from the solubility), for KCl ~0.80 (Tang, 1997), and the measured deliquescence point for K_2CO_3 is between 0.30-0.40 (when estimated from solubility: 0.54).

The IC analysis of the submicrometer flue gas particles collected in parallel with the H-TDMA RH scans showed the fine mode particles to consist of (molar fractions) 20% KCl, 37% K_2SO_4 and 42% K_2CO_3 (Figure 4, n=3). This corresponds to (dry) volume fractions of 0.14, 0.44 and 0.42.

When using the ZSR method to calculate the hygroscopic growth of a mixture consisting of KCl, K_2CO_3, and K_2SO_4, not taking solubility into account, the ZSR model predicts a water uptake that exceeds that observed with the H-TDMA (see Figure 6). Comparing the slope of the experimental RH curve to that of the pure compounds it can be seen that some compound most likely goes into solution as RH increases. Taking into account the low solubilities of K_2SO_4, and KCl in the ZSR prediction, the assumed mixture can reproduce the hygroscopic behavior of the flue gas particles surprisingly well. Since it could be seen from the PIXE analysis that the sulfur to chloride ratio was changing as a function of size (Figure 5) a calculation was also performed doubling the number of KCl at the cost of K_2CO_3. The result is then even closer to the measured hygroscopic growth. KCl goes completely into solution at a water activity of ~0.80, which can be discerned as a slight discontinuity in the calculated ZSR curve in Figure 6. At 90% RH only 10% of the K_2SO_4 is in solution.

During the time periods scanning in the RH mode, the hygroscopic behavior could thus be explained with the ZSR rule using only the inorganic compounds as main components of the particles. From the RH scans no obvious difference in hygroscopic behavior was seen between the 120 and 200 nm particles.

Size scan

Using the size-scanning mode of the H-TDMA, the hygroscopic behavior as a function of dry particle diameter was studied. For these measurements, the system was operated at 90% RH and the result is shown in Figure 7. A rather constant growth was observed, with slightly decreasing growth factors with increasing size. During the 90% RH scans the boiler load was either 50 or 100%. A trend with somewhat higher hygroscopic growth at lower load was also observed, Figure 7.

The average values for the 90 % scans were also plotted in Figure 6 together with the ZSR calculation. Here RH 90% is recalculated into water activity. Consequently, in the figure the higher activities correspond to the growth of the larger particles. The hygroscopic diameter growth is presented in Table 1.

From the PIXE analysis it was seen that the sulfur to chlorine mass ratio increased with size (Figure 5), indicating that the smaller particles had a slightly different chemical composition, e.g. a larger fraction of KCl. Using the ZSR method and taking limited solubility into account, an increased fraction of KCl would result in higher hygroscopic diameter growth at 90% RH.

As an overall result we can conclude that there was no larger fraction of elemental or insoluble organic carbon present, except from possibly in the larger sized particles. This is in agreement with the results presented in section 3.2.

Internal mixture and temporal variation

For the 1 MW boiler the humidified size distribution mainly revealed unimodal growth. The broadening (geometric standard deviation) of each humidified size distribution was slightly

larger than if the particles of one scan were perfectly internally mixed i.e. all individual particles had similar hygroscopic growth. This suggests that the processes of nucleation, condensation, and coagulation create an internally well-mixed aerosol. A measure of the variation of the hygroscopic growth factor within each scan is the interval in growth factor covering 95% of the spectrum (see section 2.2.3). For 110 nm particles the interval was ± 0.12, to be compared to that of pure ammonium sulfate (similar growth factor) is ± 0.06. The average spread in growth factor for each H-TDMA scan is presented together with the average growth in Figure 8 and Table 1. An example of a humidified size distribution at ~90 % RH of 100 nm particles is shown in Figure 9.

The standard deviation in hygroscopic growth factor over time is shown in Figure 10, indicating variations in the combustion process in time (leading to a slight variation in chemical composition), especially for the smallest and the larges particles. The temporal standard deviation of the average hygroscopic growth in time is also presented in Table 1.

3.3.2 Boiler 2: 1.5 MW pellets fired boiler

During the measurements at boiler 2 the load was more stable than for boiler 1, and was typically around 30% with temporal variations between ~20-50%. The number of scans taken during this experiment was also higher. The H-TDMA was running more stable leading to smaller estimated errors than in the previous boiler (Figure 7). Since the time resolution of one H-TDMA scan was ~3-4 minutes the fast events with high concentrations of EC was sorted out by the quality assurance procedure and no details of mixing status of single particles at these events could be determined

A different dilution system was used for the boiler 2 measurements using heated primary dilution air, resulting in a low RH throughout the sampling system before entering the instruments.

RH scan

For boiler 2 RH scans were made for 100, 200, and 300 nm particles. The concentrations were low and changed rapidly in the measurements for 200 and 300 nm particles. Therefore only few spectra passed the quality criteria.

For the 100 nm particles the RH scans showed no hygroscopic growth up to ~0.5 in a_w (water activity), Figure 11. For a_w around 0.5 and up to 0.78 a "shrinking" behavior was observed (Figure 11), with a minimum in hygroscopic growth at $a_w \sim 0.73$. For a_w higher than 0.8 the hygroscopic growth factor was >1. The shrinking behavior between a_w 0.5 and 0.78 could be explained by restructuring of the agglomerate particles into a more spherical shape while taking up only small amounts of water. Since the mobility diameter of agglomerates is larger than the volume or mass equivalent diameter, the effects of agglomerate particles shrinking when humidified between the two DMA:s would lead to an underestimation of the hygroscopic growth.

Since the particles tend to show a decrease in mobility diameter until a_w ~0.73, the particles below this water activity are not yet spherical (i.e. not a liquid droplet). At higher water activities a growth is observed which indicates that the particles above this a_w are likely to be liquid spherical droplets.

For 200 and 300 nm particles the number of accepted scans was low, as well as the hygroscopic growth. However, the particles showed the same trend with shrinking behavior and with a slight shift towards higher RH (see Figure 11).

The ZSR method was applied also for the boiler 2 measurements. The chemical composition used in the calculations was 57 % K_2SO_4 and 43 % KCl (molar fractions), estimated from the IC analysis. However, without taking into account the particle agglomerate structure the comparison to measured growth is meaningless. When using a fractal dimension of 2.49 to describe the agglomerated structure (and C_3=1.79) of the combustion particles (see details in the section below) and the limited solubility of the salts, the ZSR method can reproduce the measured growth well, as shown in Figure 11. KCl is completely in solution at 0.83 a_w. Due to the limited solubility of K_2SO_4 only 6 % of K_2SO_4 is in solution at RH 90 %. The reason for the hygroscopic growth below the deliquescence point of KCl can be explained by the presence of other compounds, not contributing much to the growth, but still providing a small liquid phase.

The RH scans performed for particles from boiler 2 clearly showed a reshaping behavior. This was not the case for boiler 1 and the difference can be attributed to the dilution system. For boiler 1, the primary diluting air was not heated, and the RH could reach the level above which reshaping occurs before entering the H-TDMA.

Size scan

Scanning DMA 1 in size at 90% RH revealed a strong decrease in hygroscopic growth as the particle size increased, from 1.46 for the 30 nm particles down 0.99 for the 350 nm particles. This decrease was observed despite the fact that the chemical composition obtained from IC

analysis as well as the S/Cl ratio obtained from PIXE data was essentially independent of particle diameter. For particles larger than 150 nm the decreasing growth might have been affected by the presence of EC (discussed in section 3.2). For particles <100 nm the size-dependent growth is likely to be caused by the fractal-like shape of the particles. From the definition of fractal dimension follows that larger particles have higher shape factors and accordingly shrink more when reshaped into spherical droplets. From the hygroscopic behavior the fractal dimension can be assessed and corrected for, as presented in a section below.

Internal mixture and temporal variation

The humidified size distribution of boiler 2 was in general narrow with a slight modal structure, see Figure 9. At some occasions, often in connection to higher loads, a very distinguishable modal structure was seen - generally clearer for the smaller sized particles. This means that the aerosol at these occasions was externally mixed, i.e. particles of the same size had different chemical composition. Examples of humidified size distributions for 100 nm particles at ~90 % RH is shown in Figure 9.

The temporal variation of the measured hygroscopic growth was prominent, but still smaller than for boiler 1. This may be explained by smaller load changes or the use of more homogeneous fuel in boiler 2 (pellets) than in boiler 1 (moist forest residue). The variation in time is presented as standard deviation of the growth factor in Figure 10 and Table 1.

Fractal dimension from H-TDMA data and correction for particle shape

From the slope in the uncorrected hygroscopic growth as a function of size, the fractal dimension of the aerosol can be estimated as described in section 2.5.1. Only particles in the

interval 30-100 nm particles were used because the chemical composition should be constant over the size range used. In the interval 30-100 nm this assumption is supported by the PIXE and IC analysis. Larger particles were not included (section 3.2) since elemental carbon was likely enriched in particles larger than about 150 nm.

The fractal dimension was estimated to 2.49 assuming that the 30 nm particles were close to the primary particle size i.e. were approximately spherical. To test the sensitivity to assumed primary particles size (i.e. absolute hygroscopic growth) the fractal dimension is extrapolated for 10 nm primary particles (equation 8, Gf=1.59). The resulting fractal dimension is then 2.47. As can be noted, the fitted fractal dimension is only weakly dependent on the absolute growth of the particles but instead essentially determined by the relative change in the measured ratio between $d_{wet}/d_{me\,dry}$. However, the constant C_3 is strongly dependent on the absolute growth.

To determine C_3 in eq.8, we had to assume the absolute hygroscopic growth, determined by the growth of the primary particle. The lower limit of the corrected hygroscopic growth is set by the growth of the 30 nm particles. Assuming that these particles are spherical C_3 is fitted to 1.79. From D_f and C_3 the corrected growth factor was calculated from equation 8. The corrected growth is shown in Figure 12. It is worth noting that if the 30 nm particles also had an agglomerated structure, the real water uptake is underestimated. The lower limit (spherical 30 nm particles) corresponds to a dynamic shape factor (equation 4) of 1.42 for the 100 nm particles and 1.65 and 1.75 for the 200 nm and 300 nm particles respectively. In Figure 12 it can be seen that when the larger particles (>150 nm) were corrected to the same fractal dimension as particles <150 nm in diameter, the larger particles had a somewhat lower growth than expected if the chemical composition were constant over size. However not as low as

expected if dominated by soot. This is either because the intermittent events with high soot concentration are sorted out by the quality assurance procedure (restrictions in the variation in concentration during one scan) or due to a different fractal behavior of these particles.

The estimated dynamic shape factors were applied also to the RH scans, to recalculate the hygroscopic growth. The recalculated growth was used in the comparison with the result from the ZSR method. The results agreed well (see previous section and Figure 11).

Pagels et al. 2005 varied the temperature in a similar ejector sampling system in a larger boiler operated with moist forest residue. They found that dried particle samples decreased their mobility diameter on average 20% when the particles experienced high RH during sampling. Larger particles shrank more than smaller ones. They estimated the fractal dimension to be ~2.5 from parallel SMPS-ELPI measurements. In that study the elemental carbon concentration was negligible. They also found that a similar restructuring process occurred at temperatures above 400 °C in experiments incorporating a thermo-desorber.

4. Summary and Conclusions

The flue gas particles emitted from two 1 and 1.5 MW biomass combustion units had, in contrast to other combustion aerosols such as diesel exhaust particles, relatively high hygroscopic growth factors. This is explained by the particle composition dominated by potassium salts (KCl, K_2SO_4, and K_2CO_3). The average diameter growth at RH=90% for 110/100 nm particles was 1.68 in boiler 1, and ~1.5 (uncorrected growth 1.24) in boiler 2.

For both boilers the particles were internally well-mixed, except at some occasions in boiler 2 when a second more hygroscopic mode appeared. The temporal variation in growth factor for the 110/100 nm particles was 0.10 (1 stdev.) and 0.07 for the two boilers respectively.

The measured hygroscopic growth could be reproduced surprisingly well by the modeled growth using ZSR method, where the chemical composition was assumed on the basis of IC and only inorganic ions were considered. A consistency between measured and modeled hygroscopic growth was found for both boilers.

Fast temporal variations in the size-spectrometer (ELPI) measurements identified as EC-enriched particles were observed for particles larger than 150 nm in the 1.5 MW boiler. These observations were consistent with filter measurements of EC/OC published previously (Wierzbicka et al. 2004) and size-resolved recovered mass fractions from ion-chromatography. The mixing status at these occasions was not known since events with fast variations were sorted out in the H-TMDA quality procedure.

In boiler 2 the hygroscopic growth appeared to decrease strongly with increasing particle size, while the chemical composition was largely independent for particle sizes in the range 30-100 nm. Further, 100 nm particles decreased their mobility diameter by around 10% at RH~75% before growing to droplets. The likely explanation for these results was that the particles changed morphology from agglomerated structures to droplets when humidified, leading to an underestimation of the water-uptake. In this study a method was developed to estimate and correct for the fractal dimension of agglomerated particles. From our H-TDMA data, the fractal dimension was estimated to ~2.5, which is somewhat higher than the value of 2.35 for diesel engines (Park et al. 2004), indicating more compact particles.

For boiler 1 no indication of agglomerate particles shape was seen. This was attributed to a different sampling system used, where the particles experienced high RH already during sampling.

Since the solubility of K_2SO_4, a salt often formed in biomass burning, is limited, it is important to take the low solubility into account when extrapolating the hygroscopic growth from water vapor sub saturations to supersaturations relevant for cloud processes or the humidity in our lungs. Estimating the number of soluble ions from the hygroscopic growth at 90% RH would lead to a significant underestimation of the hygroscopic growth since in this case at 90 % RH only ~60 % and 35 % of the particle is in solution respectively, even though the soluble volume fraction is close to 1.

The environmental importance of the observation with high hygroscopic growth of the flue gas particles is mainly related to the atmospheric residence time of the emitted particles. Hygroscopic particles are more easily incorporated in cloud and raindrops, leading to a higher probability of wet deposition and thus a shorter residence time in the atmosphere, compared to a hydrophobic particle of the same dry size. From a human health aspect, the deposition pattern of the particles in the humid environment of the human respiratory system (RH close to 99.5%) is strongly affected by the hygroscopic properties of the inhaled aerosol particles. The growth in diameter inside the lungs for 100 nm particles from both boilers would be ~4.5 leading to an increase in volume of 90 times (assuming ideal solutions). In general, a smaller number of the particles is deposited when changing from a hydrophobic to a hygroscopic combustion aerosol. On few occasions soluble volume fraction, considerably lower than 1.0,

was found. This was likely caused by organic or elemental carbon produced by incomplete combustion.

References

Andreae, M.O. and Merlet, P. (2001). Emissions of trace gases and aerosols from biomass burning, *Global Biogeochemical Cycles*, Vol.15, No. 4, 955-966.

Anselm A., Heibel T., Gebhart J. & Ferron G. (1990). Invivo Studies of Growth-Factors of Sodium-Chloride Particles in the Human Respiratory-Tract. *Journal of Aerosol Science* 21, S427-S430.

Brunner., T., Obernberger, I., Jöller. M, Arich A. and Pölt P. (2001). Behavior of ash forming compounds in biomass furnaces – Measurement and analysis of Aerosols formed during fixed-bed biomass combustion. In T. Nussbaumer (Ed.), *Aerosols from biomass combustion* (p. 75), ISBN 3-908705-00-2, Switzerland: Verenum.

Chand, D., Schmid, O., Gwaze, P., Parmar, R. S., Helas, G., Zeromskiene, K., Wiedensohler, A., Massling, A., and Andreae M. O. (2004). Laboratory measurements of smoke optical properties from the burning of Indonesian peat and other types of biomass, To be submitted in *Geophysical Research Letters*.

Christensen K.A., Stenholm M. and Livbjerg H. (1998). The formation of submicron aerosol particles, HCl and SO2 in straw-fired boilers. *Journal of Aerosol Science* 29, 421-444.

Cocker D.R., Whitlock N.E., Flagan R.C. & Seinfeld J.H. (2001) Hygroscopic properties of Pasadena, California aerosol. *Aerosol Science and Technology* 35, 637-647.

Dua, S.K., and Hopke, P.K. (1996). Hygroscopic Growth of Asorted indoor Aerosols, Aerosol Sci. Technol., 24:151-160.

Guendouzi, M. EL., Mounir, A., and Dinane, A. (2003). Water activity, osmotic and activity coefficients of aqueous solutions of Li_2SO_4, Na_2SO_4, K_2SO_4, $(NH_4)_2SO_4$, $MgSO_4$, $MnSO_4$, $NiSO_4$, $CuSO_4$ and $ZnSO_4$ at T=198.15 K, *J. Chem. Thermodynamics*, 35, 209-220.

Gysel M.,Weingartner E., Baltensperger M. (2002). Hygroscopicity of Aerosol Particles at Low Temperatures. II. Theoretical and Experimental Hygroscopic Properties of Laboratory Generated Aerosols, *Environ. Sci. Technol.*, 36, 63-68.

Hedberg, E., Kristensson, A., Ohlsson, M., Johansson, C., Johansson, P.-Å., Swietlicki, E., Vesely, V., Wideqvist, U., Westerholm, R. (2002). Chemical and physical characterization of emissions from birch wood combustion in a woodstove, *Atmospheric Environment*, 36, 4823-4837.

Hinds, W. C. (1999). Aerosol Technology, John Wiley & Sons, Inc., New York.

Intergovernmental Panel on Climate Change (IPCC) Climate change (2001). Third Assessment Report, Scientific Basis, 2001.

Jimenez S. & Ballester J. (2004) Formation and emission of submicron particles in pulverized olive residue (orujillo) combustion. *Aerosol Science and Technology* 38, 707-723.

Johansson L.S., Leckner B., Gustavsson L., Cooper D., Tullin C. & Potter A. (2004). Emission characteristics of modern and old-type residential boilers fired with wood logs and wood pellets. *Atmospheric Environment* 38, 4183-4195.

Krämer, L., Pöschl, U., Niessner, R. (2000). Microstructural rearrangement of Sodium Chloride condensation aerosol particles on interaction with water vapor, *J. Aerosol Sci.* Vol. 31, No. 6, pp. 673-685.

Köhler, H. (1936). The Nucleus in and the Growth of Hygroscopic Droplets, *Trans. Faraday. Soc.* 32, 1152-1161.

Lide, D. R. E. (1991). Handbook of chemistry and physics. 72nd edition, CRC Press.

Lillieblad L., Szpila A., Strand M., Pagels J., Rupar-Gadd K., Gudmundsson A., Swietlicki E., Bohgard M. & Sanati M. (2004). Boiler operation influence on the emissions of submicrometer-sized particles and polycyclic aromatic hydrocarbons from biomass-fired grate boilers. *Energy & Fuels* 18, 410-417.

Marjamaki M., Keskinen J., Chen D.R. & Pui D.Y.H. (2000). Performance evaluation of the electrical low-pressure impactor (ELPI). Journal of Aerosol Science 31, 249-261.

Mavrocordatos D., Kaegi R. & Schmatloch V. (2002). Fractal analysis of wood combustion aggregates by contact mode atomic force microscopy. *Atmospheric Environment* 36, 5653-5660.

McMurry, J. and Fay, R. C. (1998). *Chemistry*, 2nd ed., ISBN 0-13-737776-2.

Pagels, J., Strand, M., Rissler, J., Szpila, A., Gudmundsson, A., Bohgard, M., Lillieblad, L., Sanati M. and Swietlicki, E. (2003). Characteristics of Aerosol Particles Formed During Grate Combustion of Moist Forest Residue, *J. Aerosol science*, 34, 1043-1059.

Pagels, J., Strand, M., Dahl A., Szpila, A., Swietlicki, E., Sanati, M., Bohgard, M.. (2004). In situ measurements of particles from biomass combustion - Sensitivity of particle morphology to humidity and temperature, Submitted to *Journal of Aerosol Science.*

Park K., Kittelson D.B. & McMurry P.H. (2004). Structural properties of diesel exhaust particles measured by transmission electron microscopy (TEM): Relationships to particle mass and mobility. *Aerosol Science and Technology* 38, 881-889.

Reid, J. S., Koppmann, R., Eck, T.F., and Eleuterio, D. P. (2004). A review of biomass burning emissions, part II: Intensive physical properties biomass burning particles, *Atmos. Chem. Phys. Discuss.*, 4, 5135–5200.

Rissler, J., Swietlicki, E., Zhou, J., Roberts, G., Andreae, M.O., Gatti, L.V., Artaxo, P. (2004). Physical properties of the sub-micrometer aerosol over the Amazon rain forest during the wet-to-dry season transition – Comparison of modeled and measured CCN concentrations,

Atmospheric Chemistry and Physics, 4, 2119-2143.

Schmidt-Ott, A., Baltensperger, U., Gäggeler, H.W., and Jost, D.T. (1990). Scaling behaviour of physical parameters describing agglomerates, J. Aerosol Sci., Viol 21, No 6, 711-717.

Simoneit, B.R.T., Schauer, J.J., Nolte, C.G., Oros, D.R., Elias, V.O., Fraser, M.P., Rogge, W.F., Cass G.R. (1999). A Levoglucosan, a tracer for cellulose in biomass burning and atmospheric particles, *Atmospheric Environment* 33, 173-182.

Stokes, R. H. and R. A. Robinson (1966). Interactions in aqueous nonelectrolyte solutions: I. Solute solvent equilibria, *Journal of Physical Chemistry*, 70, 2126-2130.

Stolzenberg, M.R. and McMurry, P.H. (1988). TDMAFIT user's manual. PTL Publications No.653, Particle Technology Laboratory, Department of Mechanical Eng., University of Minnesota, Minneapolis, MN, USA.

Swedish Energy Administration (2003). Energy in Sweden, facts and figures, 2004, www.stem.se.

Svenningsson, B. (1997). Hygroscopic growth of atmospheric aerosol particles and its relation to nucleation scavenging in clouds, Doctoral dissertation at Lund University, Dep. of Nuclear physics, Lund, Sweden, ISBN 91-628-2764-2.

Svenningsson, B., Rissler, J., Swietlicki, E., Mircea, M., Bilde, M., Facchini, M.C., Decesari, S., Fuzzi, S., Zhou, J., Mønster, J., and Rosenørn, T. (2004). Hygroscopic Growth and Critical Supersaturations for Mixed Aerosol Particles of Inorganic and Organic Compounds of Atmospheric Relevance, To be submitted to ACPD.

Swietlicki, E., Zhou, J., Covert, D.S., Hämeri, K., Busch, B., Väkevä, M., Dusek, U., Berg, O.H.,. Wiedensohler, A, Aalto, P.P., Mäkelä, J., Martinsson, B.G., Papaspiropoulos, G., Mentes, B., Frank, G., Stratmann, F. (2000). Hygroscopic properties of aerosol particles in the north-eastern Atlantic during ACE-2, Tellus, 52B, 202-227.

Szpila A., Strand, M., Pagels, M., Lillieblad, L., Rissler, J., Gharibi, A., Bohgard, M., Swietlicki, E., Sanati, M. (2003). Particle Emissions from Biomass Combustion, Lund University Report, ISRN LUTMDN/TMAT-3020-SE.

Tang, I.N. and Munkelwitz, H.R. (1994). Water activities, densities, and refractive indices of aqueous sulfates and sodium nitrate droplets of atmospheric importance, *J. Geophys. Res.*, Vol. 99, 18801-18808.

Tang, I. N. (1997). Thermodynamic and optical properties of mixed-salt aerosols of atmospheric importance, *J. Geophys Res.*, Vol. 102, No D2, 1883-1893, January 27.

Valmari T., Lind T.M., Kauppinen E.I., Sfiris G., Nilsson K. & Maenhaut W. (1999). Field study on ash behavior during circulating fluidized-bed combustion of biomass. 1. Ash formation. *Energy & Fuels* 13, 379-389.

Wang, S. C., and Flagan, R. C. (1989). Scanning Electrical Mobility Spectrometer, *J. Aerosol Sci.* 20(8):1485-1488.

Weingartner, E., Burtscher, H., Baltensperger, U. (1997). Hygroscopic properties of carbon and diesel soot particles, *Atmos. Env.*, Vol 31, No. 15.

Vestin, A., Swietlicki, E., Rissler, J., Zhou, J., Frank, G. (2004). CCN closure study for Amazonian dry season biomass burning aerosol, *Proc of EAC 2004.*

Winklamyr, W., Reischl, G. P., Lindner, A. O., Berner, A. (1991). A new electromobility spectrometer for the measurement of aerosol size distributions in the size range from 1 to 1000 nm, *J. Aerosol Sci.*, 22 (3), 289-296.

WHO, 2003, Report on a WHO working group (2003). Health aspects of air pollution with particulate matter, ozone and nitrogen dioxide. Copenhagen, WHO Regional Office for Europe, 2003, document EUR/03/5042688.

WHO, 2004, Report on a WHO working group (2004) Meta-analysis of time-series studies and panel studies of particulate matter (PM) and ozone (O_3). Copenhagen, WHO Regional Office for Europe, document EUR/04/5042688.

Wierzbicka, A., Lillieblad, L., Pagels, J., Strand, M., Gudmundsson, A., Gharibi, A., Swietlicki, E., Sanati M., and Bohgard, M. (2004). Particle emissions from district heating units operating on three commonly used biofuels, *Atmospheric Environment,* Vol/Issue 39/1 pp.139-150.

Zhou, J. (2001). Hygroscopic properties of atmospheric aerosol particles in various environments, Doctoral dissertation, at Lund University, Dep. Of Nuclear physics, Lund, Sweden, ISBN 91-78 4-120-3.

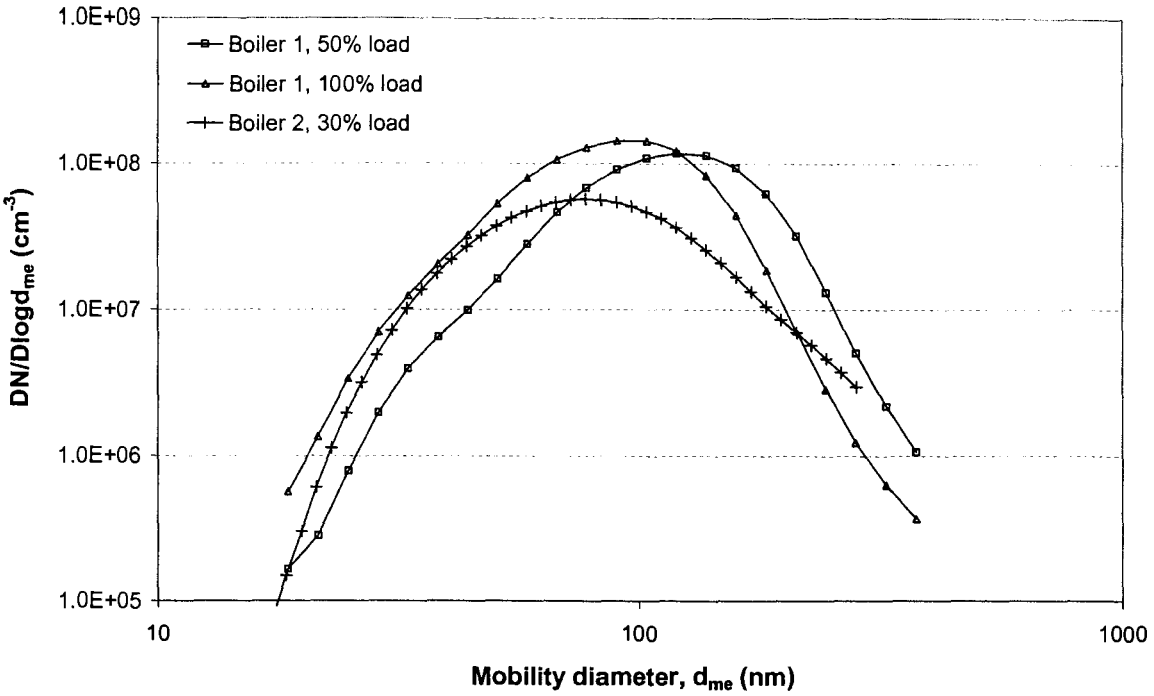

Figure 1. Number size-distributions in the two boilers.

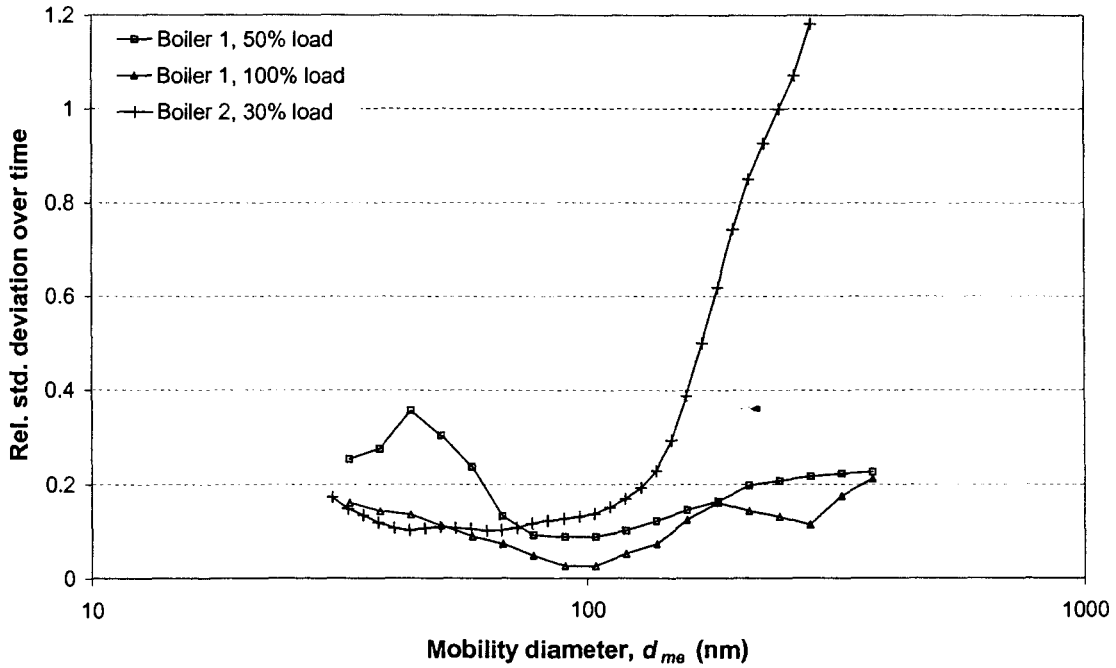

Figure 2. Relative standard deviation over time for each size-channel.

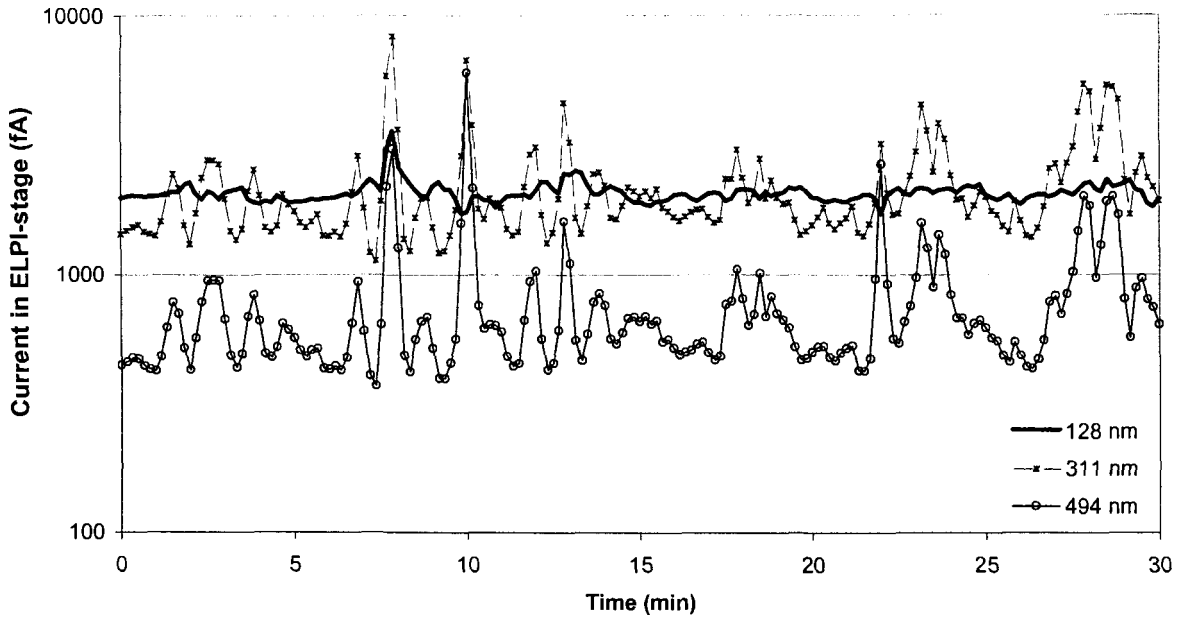

Figure 3. Representative sample of time variations in stages 3, 5 and 6 in the ELPI-impactor. Concentrations given as the current detected in each stage.

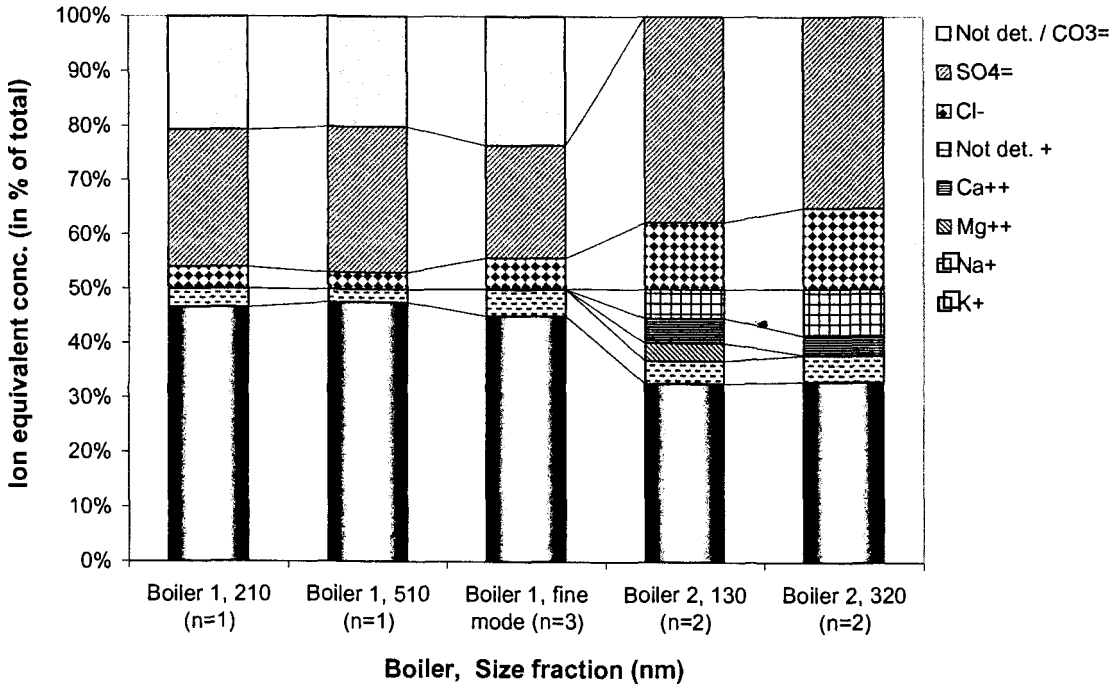

Figure 4. The result from IC-analysis. Each bar is represents an average value taken of n filters. Some variability in time and size is illustrated.

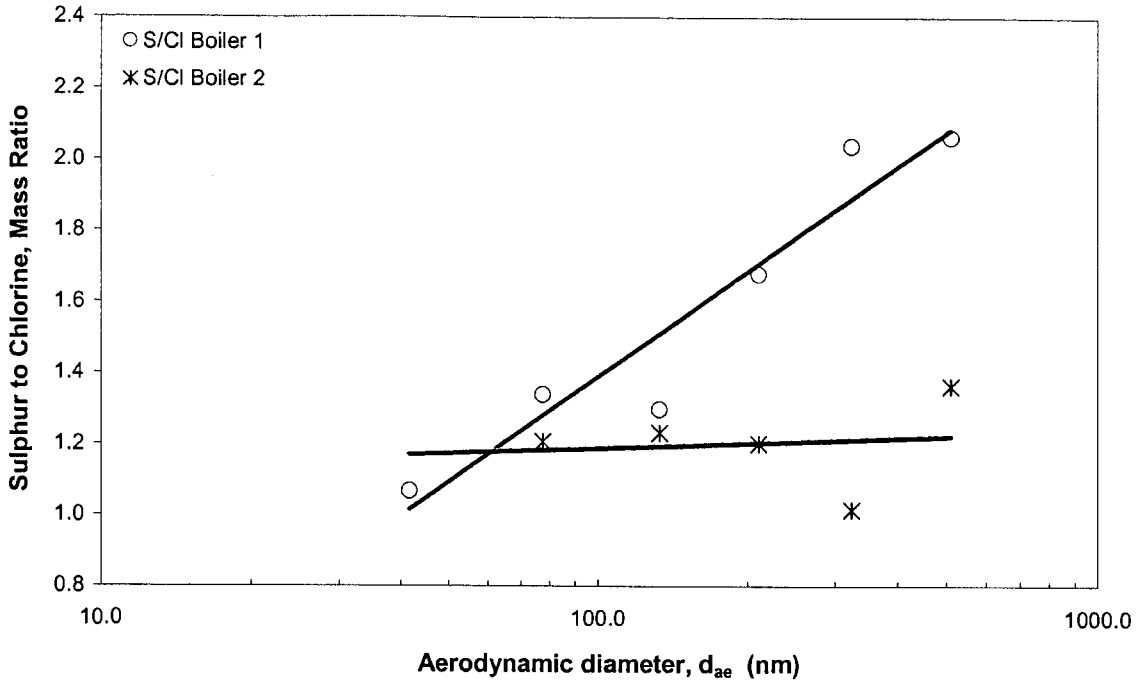

Figure 5. Size-resolved sulfur to chlorine mass ratio from the PIXE-analysis.

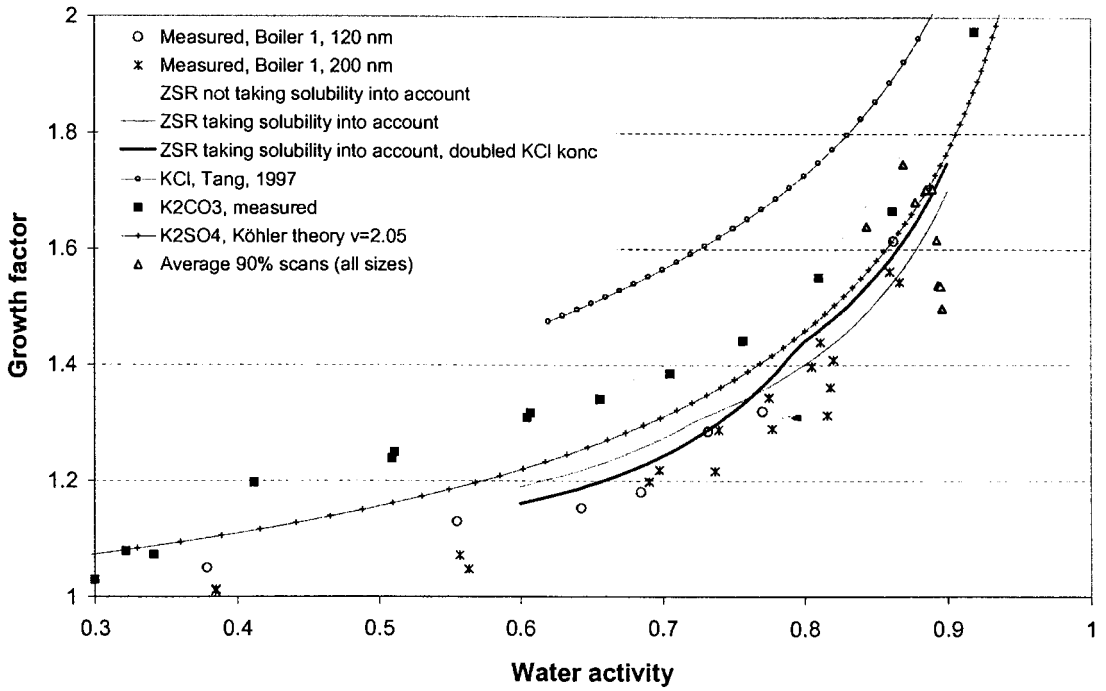

Figure 6. RH scans for boiler 1 together with calculated growth according to the ZSR mixing rule. Chemical composition based on IC analysis on filter samples. Also the growth of the pure compounds is shown.

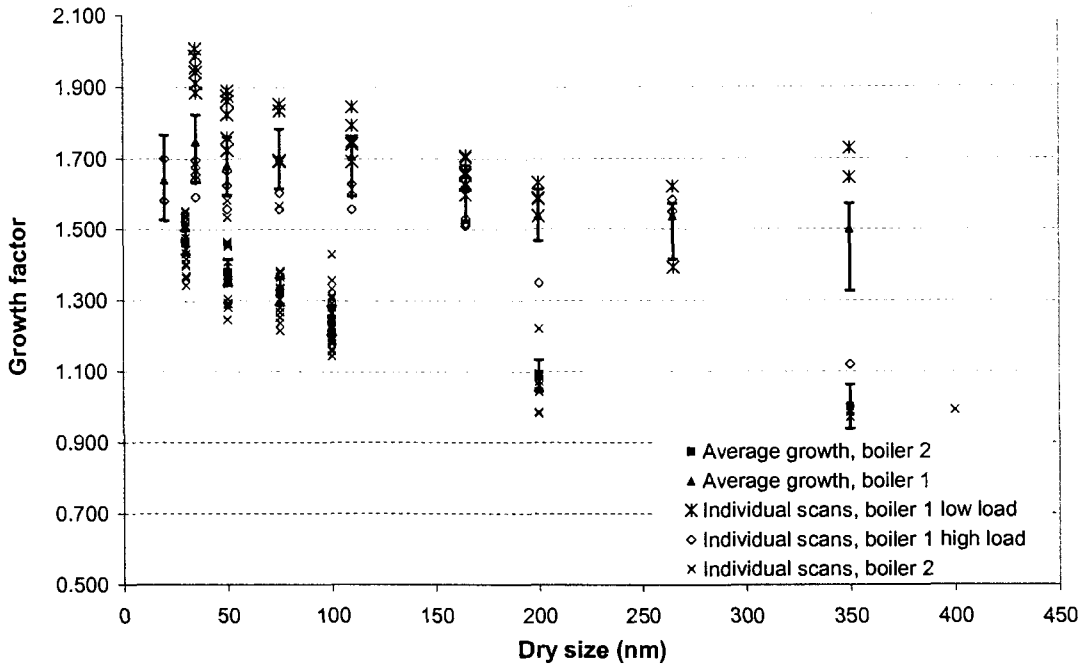

Figure 7. The hygroscopic growth, individual scans and average values. The time serie for boiler 1 is divided into high and low load. Error bars correspond to the estimated instrumental error. The larger error bars in boiler 1 are due to a larger uncertainty in RH during this measurement.

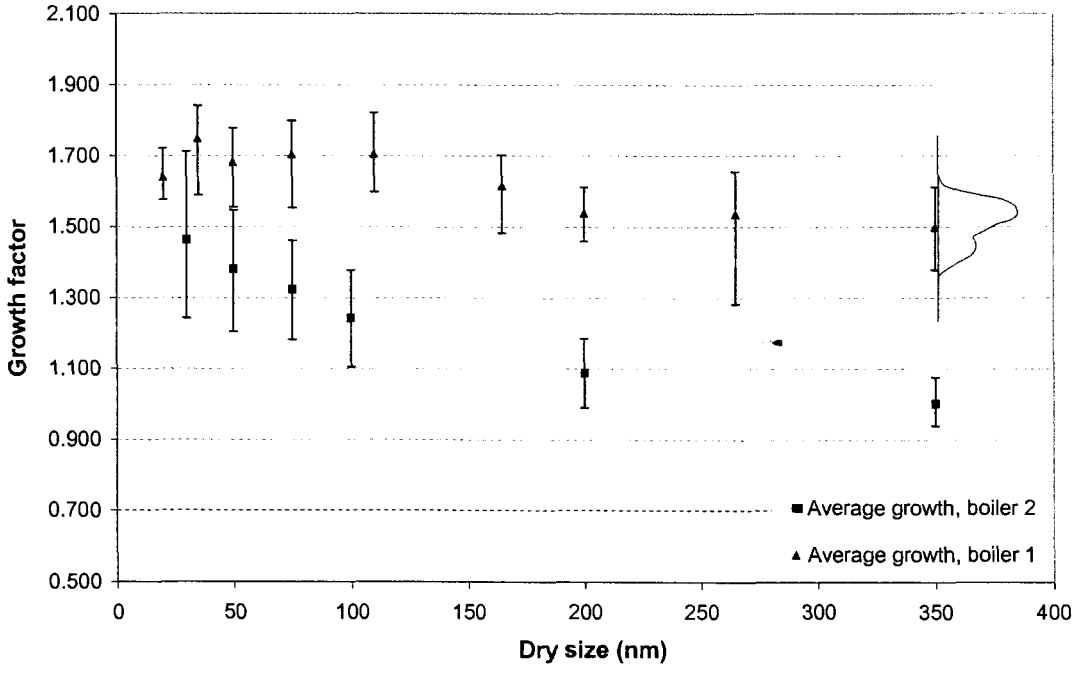

Figure 8. Average hygroscopic growth with average broadening of each individual spectra covering 90% of a spectrum (se description in the text). An illustration of how a spectrum could look like for 350 nm particles at the given broadening is given for boiler 1.

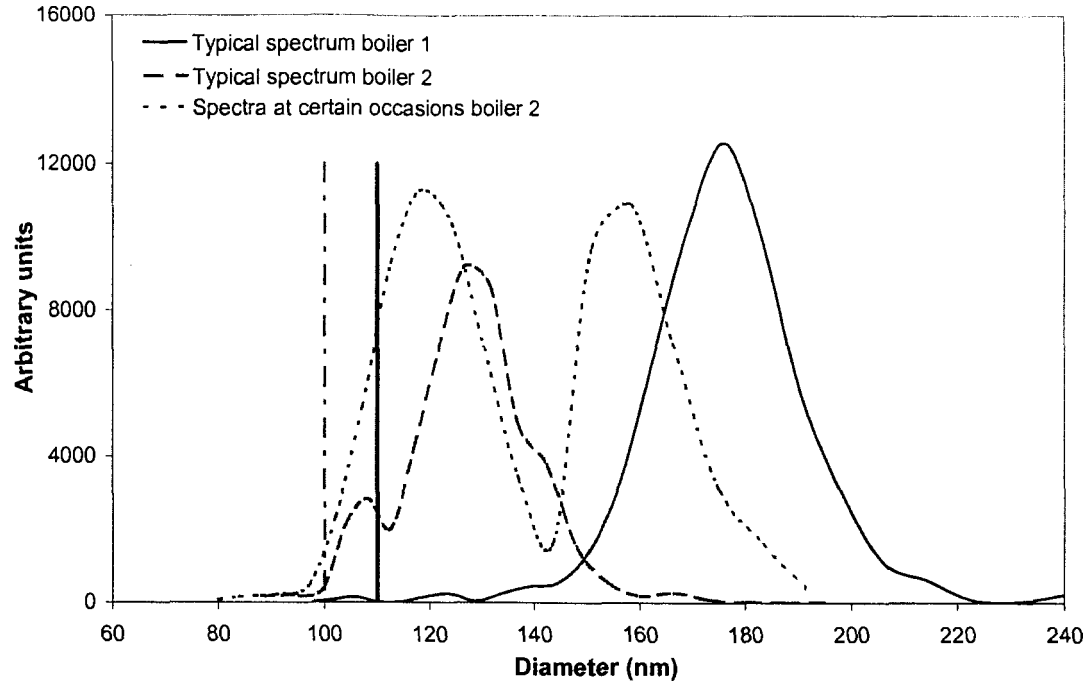

Figure 9. Example of typical humidified size distributions of a quasi monodisperse aerosol. The size distributions were often relatively narrow but occasionally a bimodal hygroscopic growth appeared indicating a clearly external mixture. The selected dry sizes were 110 nm for boiler 1 and 100 nm for boiler 2, indicated with a bar in the figure.

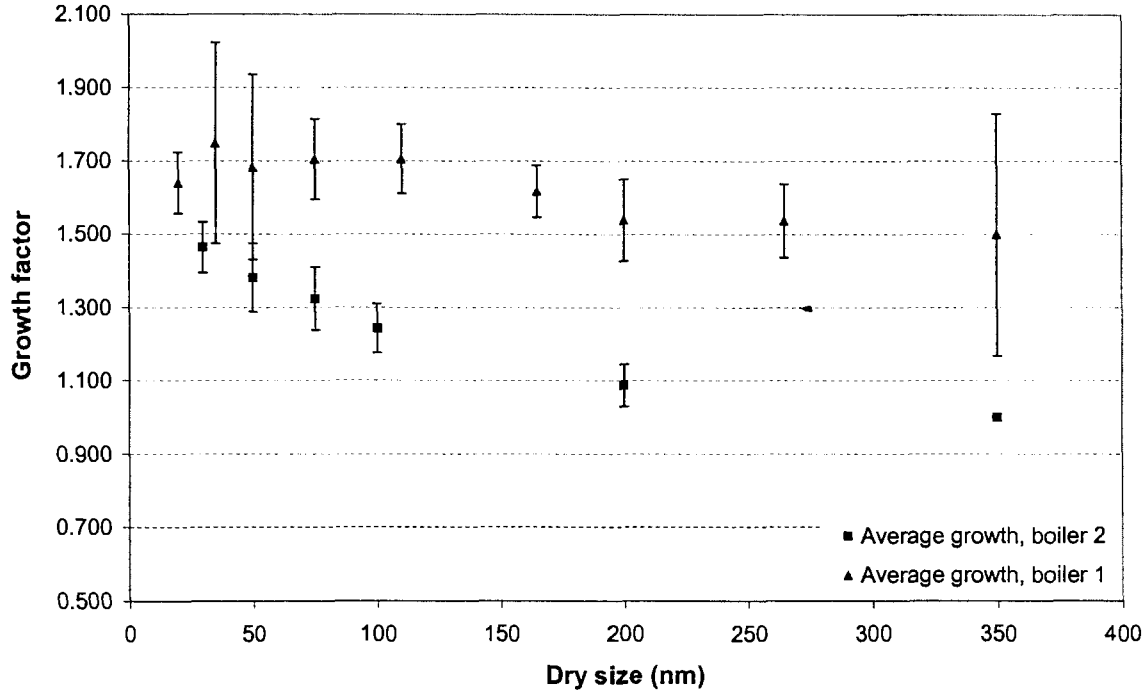

Figure 10. Average hygroscopic growth. Error bars correspond to the standard deviation of the temporal variation in growth.

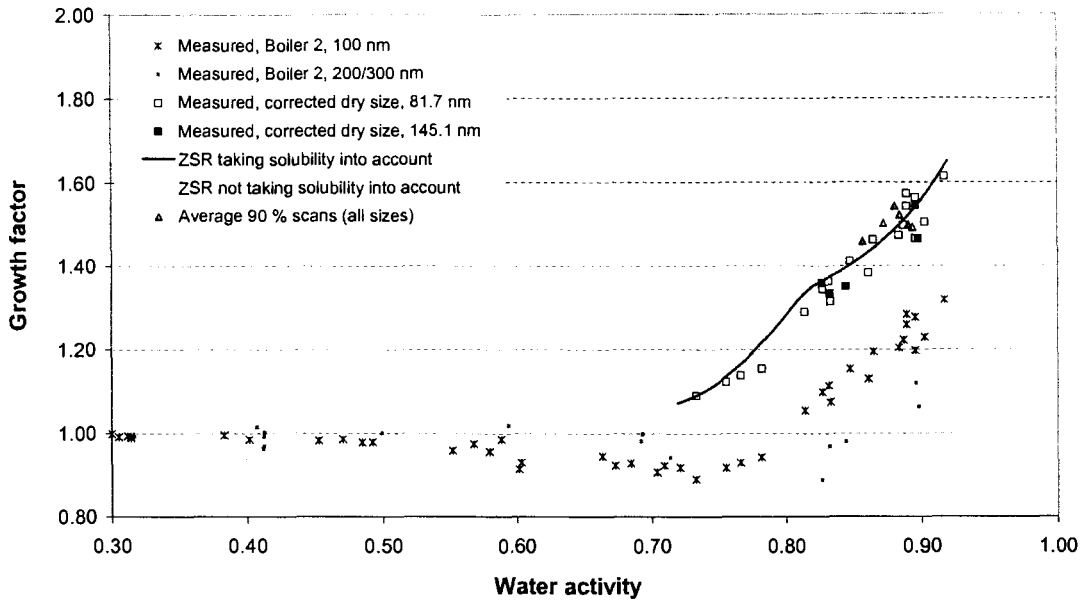

Figure 11. RH scans for boiler 2, original data as well as data corrected with respect to fractal shape. The calculations made by the ZSR mixing rule is based on chemical composition from IC analysis on filter samples.

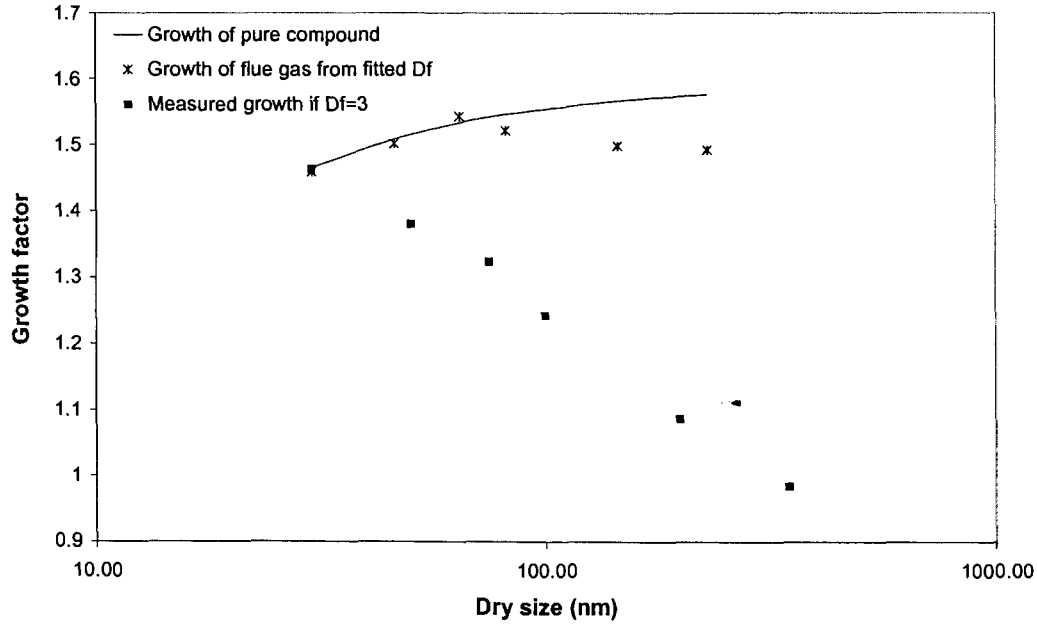

Figure 12. Size scans, boiler 2, showing both uncorrected growth as well as growth compensated for fractal like shape according to a fitted dynamic shape factor of 2.5. The 30 nm particles are here assumed to be spherical. The solid line shows the theoretical growth of a compound (having the same growth as the 30 nm particles).

Table 1 Hygroscopic properties of boiler 1 and 2.

	Dry particle diameter							
	35 nm	50 nm	75 nm	110 nm	165 nm	200 nm	265 nm	350 nm
Boiler 1								
Total number of observations	12	10	7	9	11	5	4	3
Average growth factor at 90% RH	1.72	1.68	1.70	1.68	1.60	1.54	1.48	1.50
Confidence	+ 0.09	+ 0.09	+ 0.09	+ 0.12	+ 0.09	+ 0.07	+ 0.12	+ 0.11
interval 90%	–0.16	–0.13	–0.15	–0.11	–0.14	–0.08	–0.25	–0.12
Temporal variation (1s.d.)	±0.25	±0 24	±0.10	±0.10	±0.09	±0.11	±0.12	±0.33
	30 nm	50 nm	75 nm	100 nm	200 nm	350 nm		
Boiler 2								
Total number of observations	18	17	15	25	10	3		
Average growth factor at 90% RH	1.46	1.38	1.32	1.24	1.09	0.99		
Dynamic growth factor	1	1.17	1.32	1.42	1.65	1.79		
Corrected average growth (lower limit)	1.46	1.50	1.54	1.52	1.50	1.49		
Confidence	+ 0.25	+0.17	+0.14	+0.10	+0.07	+0.01		
interval 90%	-0.22	-0.18	-0.14	-0.10	-0.06	-0.01		
Temporal variation (1s.d.)	±0.07	±0.09	±0.09	±0.07	±0.06	±0.01		